# Supplemental Information

## SUPPLEMENTAL FIGURES

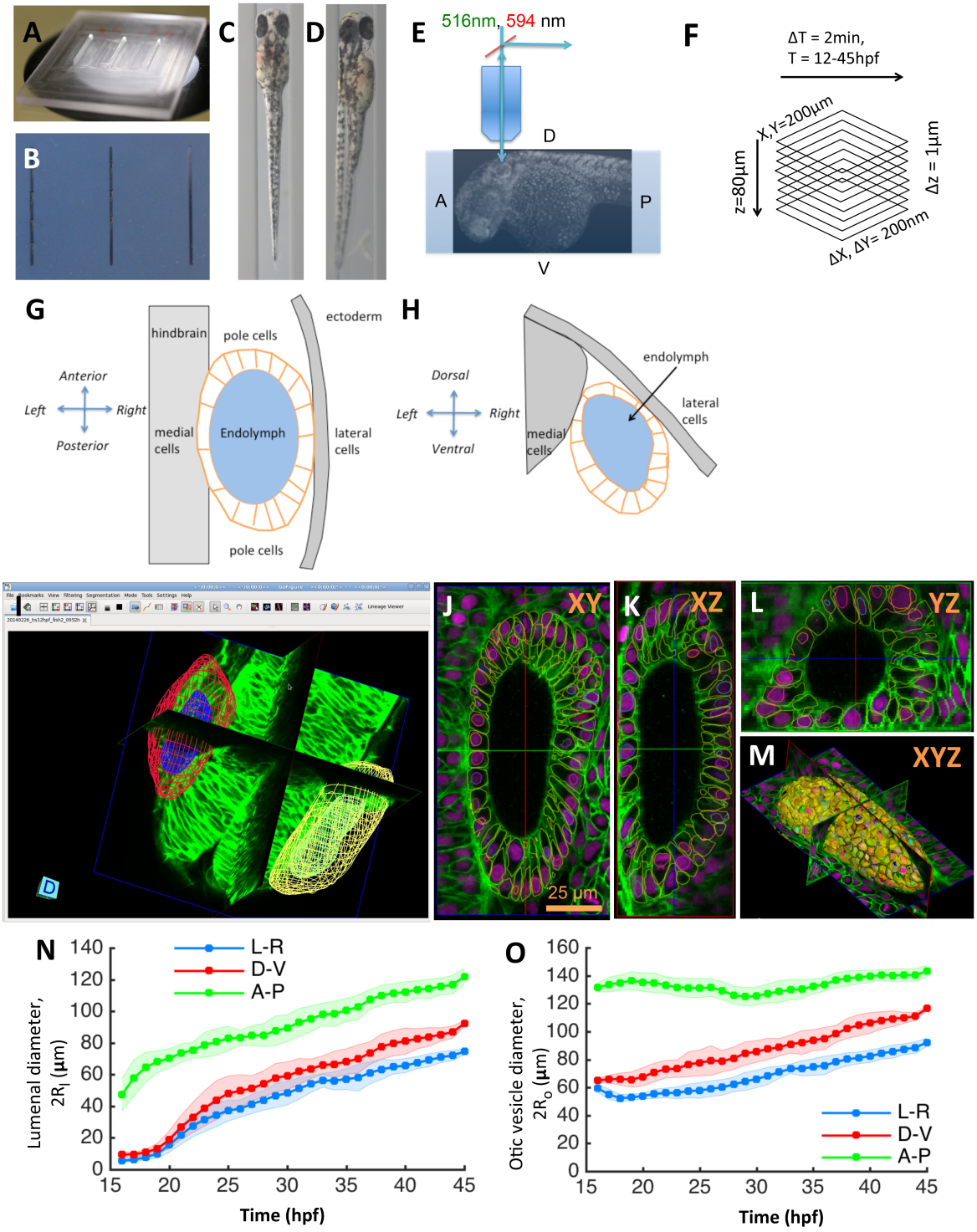

**Figure S1: Related to Figure 1. Zebrafish inner ear growth dynamics can be quantified using *in toto* imaging protocols. (A)** A "canyon" template made of plexiglass with each canyon being 1.5 mm deep and 0.4 mm wide. **(B)** 1% agarose molds are cast using the template. Rows of zebrafish embryos from 16-45 hpf stages can be mounted in orientations that position the inner ear closest to the cover-slip for imaging. **(C)** Embryos are mounted in a dorsal orientation for imaging both ears simultaneously using a 20X, 1.0 NA objective. **(D)** Embryos are mounted in a dorsolateral orientation for obtaining higher-quality images (otic tissue depth along the path of light is minimized) using a 40X, 1.2 NA objective. **(E)** Transgenic zebrafish embryos expressing bright nuclear and membrane-specific fluorescent reporters are imaged using a confocal microscope in a time-lapse mode. Embryos are (Tg(actb2:Hsa.H2B-tdTomato)hm25; Tg(actb2:mem-citrine)hm26). **(F)** The acquired images typically cover a field-of-view of $200\times200\times80\ \mu m$. With a sampling of $0.2\times0.2\times1.0\ \mu m$, image dimensions are $1024\times1024\times80$. In timelapse experiments, images are acquired every 2 minutes covering a developmental time-window ranging 12-45 hpf. **(G-H)** Diagram illustrating the standard (G) dorsal and (H) transverse views of the otic vesicle organ as indicated by the embryonic coordinate axis. The otic vesicle (orange) is situated in between the hindbrain and ectoderm tissues. The locations of the medial, lateral, and pole cell regions is as shown. **(I-L)** *In toto* images can be automatically processed using membrane and nuclei segmentation algorithms for estimating cell numbers, cell shapes, and protein expression at a single-cell resolution. Using GoFigure2, an open-source software for visualization, editing, and integrative analysis of *in toto* data, the segmentation meshes and tracks can be visualized along orthogonal image planes as shown in (I) XY, (J) YZ, (K) XZ, and as (L) triplanar 3D view. **(M)** Organ size and shape can be semi-automatically or manually processed by placing 2D contours along image planes in the GoFigure2 software platform. The software reconstructs surfaces from contours and computes volumes and surface areas. **(N-O)** Principal diameters of the lumenal cavity (N, $2R_l$) and otic vesicle (O, $2R_o$) quantified during growth show the vesicle is elongated along the anteroposterior axis while being approximately symmetric about left-right and dorsoventral axes. The principal diameters monotonically increase during growth and remain correlated. Error bars are SD.

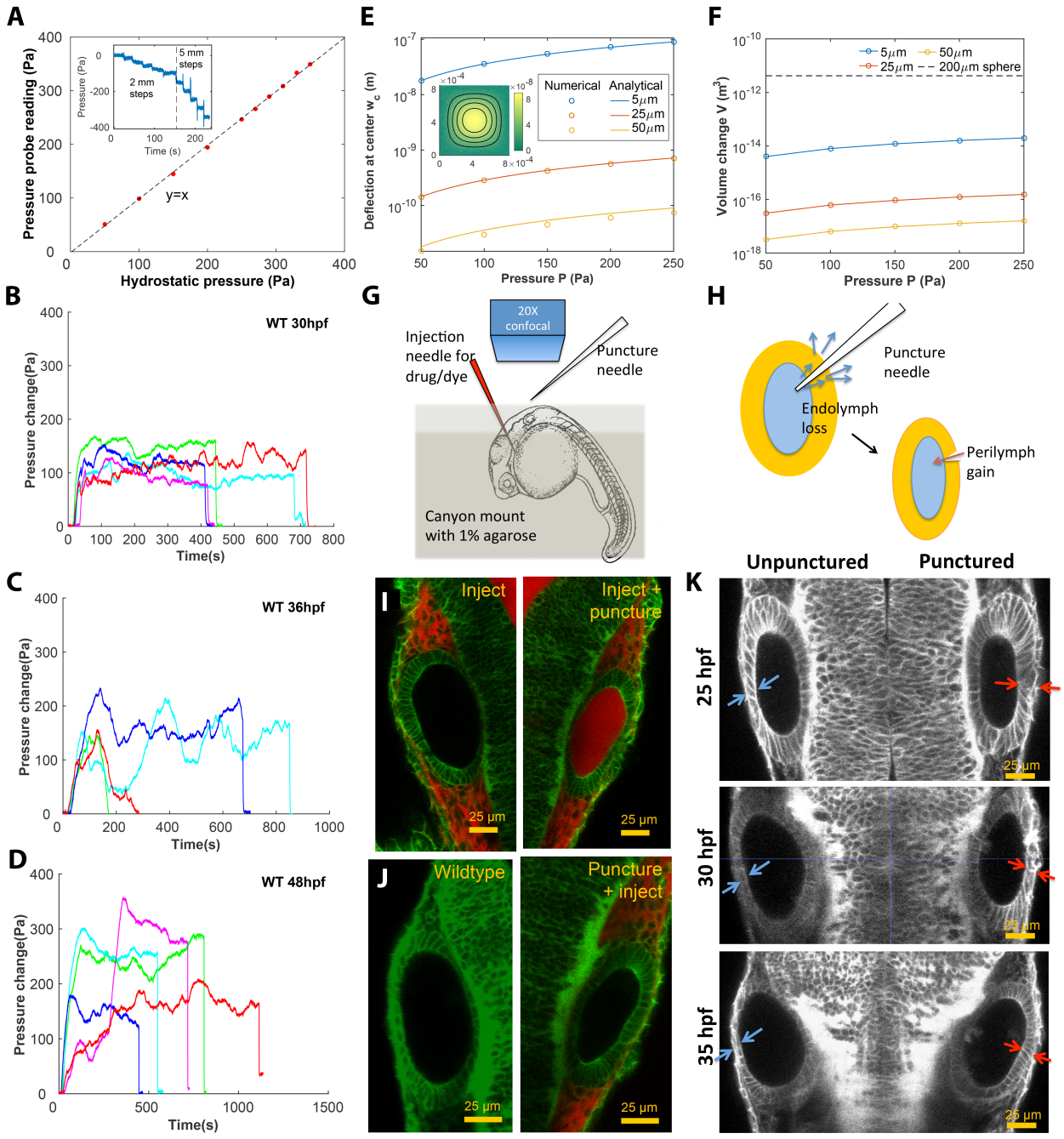


**Figure S2: Related to Figure 3. Press probe calibration and readings. (A)** The fabricated pressure probe was calibrated with hydrostatic pressure by reducing the submersion depth stepwise (inset, 1 mm$H_2O$ = 9.8 Pa), which demonstrated good linearity. **(B-D)** Pressure was measured in otic vesicle at 30 hpf **(B)**, 36 hpf**(C)**, and 48 hpf**(D)**. Presented trajectories were live readings from embryos immobilized with $\alpha$-bungarotoxin protein. n=5 for each developmental stage. **(E-F)** Calculations of membrane deformation on the piezoresistive sensing element. Colors represent different membrane thickness. **(E)**The numerical results are compared against analytical solutions for the deformation at the membrane center. (Inset)A selected solution is shown for a 5 μm membrane under 250 Pa pressure. The corresponding volume changes are shown in**(F)**, and the volume of a 200 μm diameter sphere is plotted in dotted line as a reference. **(G)** Embryos are mounted in a canyon mount made with 1% agarose for confocal imaging of left

and right vesicles with a 20X objective. Drugs or dyes are injected into the cardiac chamber and get distributed rapidly throughout the embryo including the perilymph surrounding the ear. **(H)** Schematic showing the route of lumenal fluid loss upon puncture and movement of dye from perilymph into the lumen. **(I)** 2.3 nl of 0.5 mM Alexa Fluor 594 tracer dye injected into the cardiac chamber at 30 hpf. The dye enters the circulation and is found to accumulate in the perilymph regions surrounding the vesicle. Puncturing of otic vesicle causes the dye to leak into the lumenal cavity. **(J)** Injection of dye five minutes post-puncture restricts dye transport to the perilymph, thus demonstrating the rapid sealing property of the otic tissue. **(K)** 2D confocal micrographs showing ear pairs in embryos with unilateral puncture of the right ear and staged at 25, 30, and 35 hpf. Cell shape change in unpunctured and punctured ears are highlighted using blue and red arrows respectively. Progressively through time, puncturing causes smaller transitions in cell shapes between ear pairs.

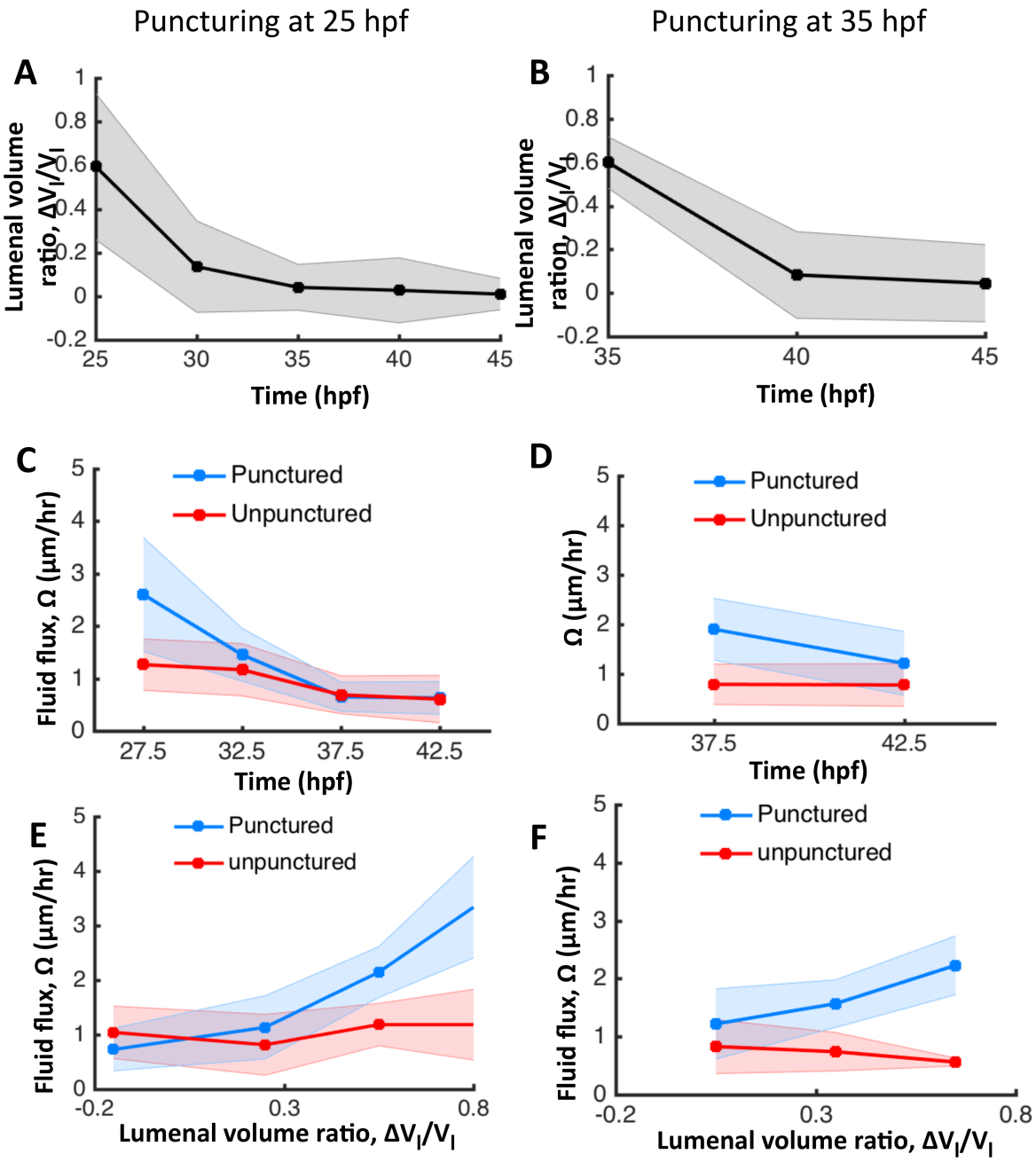


**Figure S3: Related to Figure 4. The otic vesicle regenerates to stage-specific volumes when punctured between 25-45 hpf.** In additional to experiments at 30 hpf reported in Figure 4, puncturing was conducted at 25 hpf (A, C, E) and 35 hpf (B, D, F). **(A-B)** Volume regeneration and establishment of contralateral symmetry after unilateral puncturing. The y-axis plots the difference in lumenal volumes normalized to the unpunctured volume ($\frac{\Delta V_l}{V_l} \sim \frac{\Delta R}{R}$). **(C-D)** Lumenal fluid flux Ω in punctured (blue) and unpunctured (red) vesicles during regeneration showing the increase in Ω in punctured embryos and gradual decay to the unpunctured levels. **(E-F)** Plot showing Ω as a function of $\frac{\Delta V_l}{V_l}$. The data was pooled across multiple embryos for the punctured (blue) and unpunctured (red) ears throughout their regeneration period until 45 hpf. Ω in punctured ears (blue) is positively correlated with $\frac{\Delta V_l}{V_l}$ while unpunctured ears (red) continued growing with an approximately constant flux.

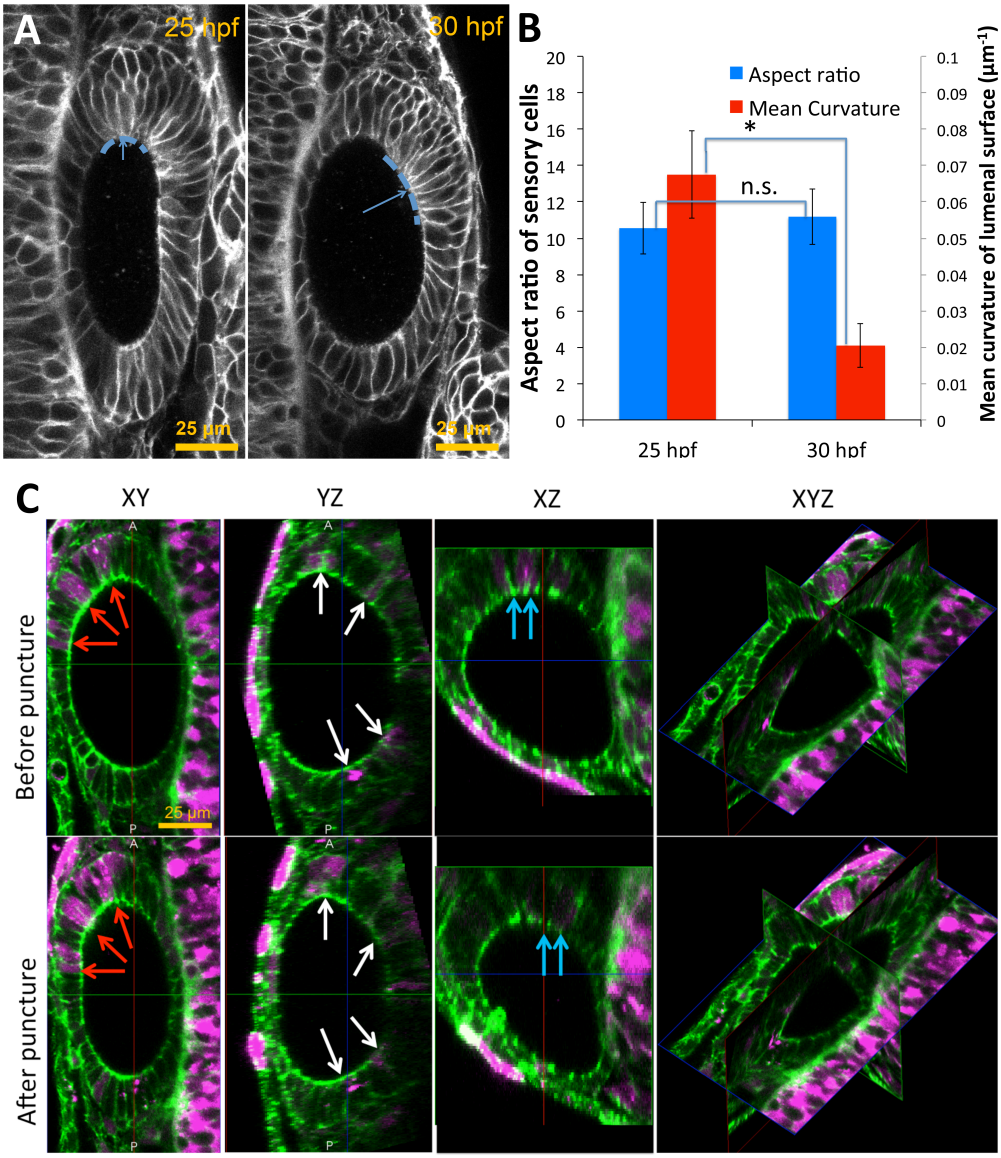


**Figure S4: Related to Figure 6. Pole cells retain their aspect ratios as they move from high to low-curvature tissue regions between 25-30 hpf. (A)** Pole cells are tracked from 25 hpf (left) to 30 hpf (right) as they treadmill from high-curvature to low-curvature (dashed blue curves) tissue regions. Mean curvature of the lumenal surface is used as a measure of the local curvature. **(B)** Quantification of the cell aspect ratios and mean curvature shows that cells retain their shapes independent of the location on the lumenal surface (n=10, $^{**}p<5.0e-5$). Error bars are SD. **(C)** For the measurement of single-cell data on shape deformations in Fig. 7I, mosaically labeled cells were tracked in Tg(actb1:GFP-utrCH) before and after puncture. Dextran TexasRed was injected into a single blastomere of 16-cell stage embryos for tracking positions of cells before and after puncture. Confocal 3D image datasets were collected before and after puncture and co-registered. The confocal micrographs show XY, YZ, XZ, and a 3D triplanar view centered on the otic vesicle of a single embryo staged at 30 hpf before (top) and after puncture (bottom). Cells positive for TexasRed fluorescence (examples shown in red, blue, and white arrows) were matched before and after puncture. For each cell, the deformation and fluorescence localization were manually measured using the GoFigure2 software.

## SUPPLEMENTAL MOVIES

**Movie S1: Related Figure 1. 2D+time confocal movie of zebrafish otic development.** Labelling by (*Tg(actb2:Hsa.H2B-tdTomato)$^{hm25}$*; *Tg(actb2:mem-citrine)$^{hm26}$*) from 12-32 hpf. Each frame has a spatial-sampling of 0.2$\mu m$ with temporal-sampling of 2 min across frames. The movie shows the formation of the otic placode (12 hpf), polarization and epithelialization of the otic vesicle (12-16 hpf), lumenization (16hpf), and subsequent growth. Both initial lumenogenesis (12-16hpf) and growth (16-45 hpf) phases are accompanied by frequent cell division events. Cells divide by moving apically and re-integrating into the epithelium. At the same time, cells appear to shrink in volume as numbers increase. During growth, cells change shape into a squamous form that coincide with the accumulation of lumenal fluid. Cell shape change is non-uniform across the medial (squamous) and pole cells (columnar). Concomitantly, deformations in the adjacent hindbrain and ectoderm tissue are visible.

**Movie S2: Related to Figure 4. 2D+time confocal movie of zebrafish otic vesicle regeneration from puncture.** Labelling by (*Tg(actb2:Hsa.H2B-tdTomato)$^{hm25}$*; *Tg(actb2:mem-citrine)$^{hm26}$*) from 27-33 hpf. Each frame has a spatial-sampling of 0.4 $\mu m$ along X-Y axis, 1.0 $\mu m$ along the Z-axis, and with temporal-sampling of 5 min across frames. The movie shows the transverse (XZ) and saggital (XY) views. The right vesicle of the embryo was punctured prior to imaging. At the start of the imaging session, the right ear is significantly smaller that the left ear. The movie shows the rapid regeneration of the right vesicle to a developmentally appropriate size, as depicted by the left ear (control). At the end of the imaging session, both the ears are similar in size.

**Movie S3: Related to Figure 5. 2D+time confocal movie showing growth and regeneration inhibition from ouabain treatment.** Labelling by (*Tg(actb2:Hsa.H2B-tdTomato)$^{hm25}$*; *Tg(actb2:mem-citrine)$^{hm26}$*) from 30-34 hpf. Each frame has a spatial-sampling of 0.4 $\mu m$ along X-Y axis, 1.0 $\mu m$ along the Z-axis, and with temporal-sampling of 5 min across frames. The movie shows the transverse (XZ) and saggital (XY) views. The embryo was soaked in 100$\mu M$ ouabain to inhibit $Na^+$-$K^+$-ATPase. The right vesicle of the embryo was punctured prior to imaging. At the start of the imaging session, the right ear is significantly smaller that the left ear. Throughout the imaging session, regular growth in the left ear and regeneration of the right ear are completely inhibited.

**Movie S4: Related to Figure 6. Spatiotemporal dynamics of F-actin localization.** A 2D+time confocal movie of zebrafish otic development from 12-32 hpf using *Tg(actb1:GFP-utrCH)* embryos that depict the localization of F-actin. Each frame has a spatial-sampling of 0.2$\mu m$ with temporal-sampling of 2 min across frames. The movie shows the formation of the otic vesicle (12-16 hpf) with apical localization of F-actin in cells. During growth (16-22hpf), F-actin is found to localize to apicolateral junctions between cells. In addition, mediolateral cells relatively lose their F-actin expression levels compared to cells at the sensory poles.

**Movie S5: Related to Figure 6. Spatiotemporal dynamics of Myosin II localization.** A 2D+time confocal movie of zebrafish otic development from 12-32 hpf using *Tg(actb1:myl12.1-GFP)* embryos depict Myosin II localization dynamics. Myosin II localization is expectedly correlated with that of F-actin (Movie S4). Each frame has a spatial-sampling of 0.2$\mu m$ with temporal-sampling of 2 min across frames.

**Movie S6: Related to Figure 6. Vesicle shape deforms upon treatment with Cytochalasin D drug at 25 hpf.** A 2D+time confocal movie of zebrafish otic vesicle was captured at 25 hpf using *Tg(actb1:myl12.1-GFP)* embryos treated with 100$\mu$M of Cytochalasin D drug. The vesicle is found to dramatically reduce Myosin II apical expression levels and change its DV/LR dimensions compared to the AP dimension. The red lines indicate dimensions at the start of the movie for comparison. Each frame has a spatial-sampling of 0.2$\mu m$ with temporal-sampling of 1 minute across frames for a total of thirty minutes.

**Movie S7: Related to Figure 6. Vesicle fails to grow upon treatment with Cytochalasin D drug at 20 hpf.** A 2D+time confocal movie of zebrafish otic vesicle was captured at 20 hpf using *Tg(actb1:myl12.1-GFP)* embryos treated with 100$\mu$M of Cytochalasin D drug. The vesicle is found to dramatically reduce Myosin II apical expression levels and growth is inhibited.